Colloids and Surfaces A: Physicochemical and Engineering Aspects 737 (2026) 139868

Contents lists available at ScienceDirect

Colloids and Surfaces A: Physicochemical and Engineering Aspects

journal homepage: www.elsevier.com/locate/colsurfa

Physicochemical characterization of hydrochar from polyurethane foam waste: Assessing the role of processing parameters

Benedetta Ciuffi [a], Edoardo Cipriani [a], Emiliano Fratini [a,b], Jesús Arauzo [c], Luca Rosi [a,*]

[a] Department of Chemistry "Ugo Schiff", University of Florence, Via della Lastruccia 3-13, Sesto Fiorentino I-50019, Italy
[b] Center for Colloid and Surface Science (CSGI), University of Florence, Via della Lastruccia 3, Florence 50019, Italy
[c] Thermochemical Processes Group (GPT), Aragon Institute for Engineering Research (I3A)Universidad de Zaragoza, Mariano Esquillor S/N, Zaragoza 50018, Spain

HIGHLIGHTS

- Hydrothermal treatments were applied to recycle rigid polyurethane foam waste.
- The operating parameters strongly influence hydrochar yields and properties.
- An inverse relationship is observed between severity values and hydrochar yields.
- Hydrochar has potential applications as nitrogen doped material and solid fuel.
- Organic phase is rich in compounds with potential applications as chemicals.

GRAPHICAL ABSTRACT

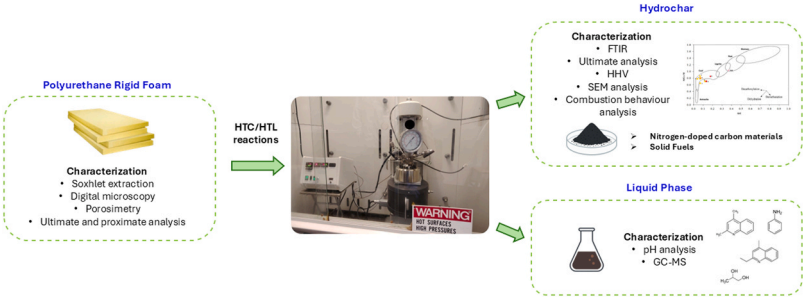

ARTICLE INFO

Keywords:
Rigid polyurethane foam
Hydrothermal treatments
Hydrochars
Nitrogen-doped carbon materials
Solid fuels

ABSTRACT

Polyurethane foams are widely used polymers. Their end-of-life is largely managed through landfilling and incineration, causing environmental concerns and resource loss. Hydrothermal carbonization and hydrothermal liquefaction have recently emerged as promising thermochemical approaches to valorise polyurethanes waste into value added products. This study presents a systematic investigation of the effects of operating parameters on hydrochars (HCs) yields and properties, using a rigid polyurethane foam as feedstock. Product yields were rationalized using the Severity Value (SV) parameter and the obtained HCs were characterized by ultimate analysis, FTIR, SEM and thermogravimetric analysis. An increase in SV led to a reduction of HCs yields, whereas the effect of the feedstock to solvent ratio exhibited only a minor influence. Ultimate analysis revealed decreased H/C and O/C ratios in all HCs, while the nitrogen content increased in all samples compared to PUR, suggesting their potential application as nitrogen-doped carbon materials. All produced HCs exhibited HHVs higher than that of PUR (27.59 MJ/kg), indicating energy densification. The calculated combustion parameters indicated that HCs exhibit lower reactivity and a slower, more controlled combustion process compared to PUR. These results together with their positioning in the coal-like regions of the Van Krevelen diagram, suggest their potential use as solid fuels. The liquid phases recovered for each test were rich in value-added compounds, including aromatic heterocycles. Overall, these findings offer valuable insights for advancing circular economy strategies in PUR waste management, highlighting the potential of HTC and HTL to simultaneously produce energy-dense solid fuels and value-added platform chemicals.

* Corresponding author.
E-mail address: luca.rosi@unifi.it (L. Rosi).

https://doi.org/10.1016/j.colsurfa.2026.139868
Received 5 December 2025; Received in revised form 27 January 2026; Accepted 4 February 2026
Available online 6 February 2026

1. Introduction

Polyurethanes (PUs) are one of the high consumption commodity polymers [1], and their world production in 2023 has reached 21.93 Mt [2]. Polyurethanes are synthesised through a polyaddition reaction between an isocyanate and polyols both with a functionality of at least 2 [3], producing carbamate groups, commonly called urethane groups. Their enormous success and use on the market are linked to their easy synthesis process, which can be carried out at room temperature and under non-severe conditions. Depending on the nature of the building blocks and the additives used, a wide range of products can be obtained such as coatings, adhesives, construction materials, paints, elastomers, furniture, and synthetic leather [4]. Polyurethane foams (PUFs) dominate the PU market, accounting for 67 % of global consumption [5]. Solid foams can be defined as binary component materials which contain a continuous phase (solid matrix) and a disperse phase (gas). The structure of most foams originates the growth of gas bubbles in the polymer matrix [6]. Blowing agents play a key role in forming the cellular structure of PUFs and are commonly classified as physical or chemical. The first ones include low-boiling point solvents such as pentane, acetone, or hexane which expand the polymer matrix by vaporization, instead the second one includes molecules such as water, that reacting with PUs building block, produce CO_2 which expands the polymer [5].

PUFs market can be divided into three main groups: flexible PU, rigid PU (PUR) and spray PU foams [6]. Flexible foams are widely used in furniture (e.g., mattresses), whereas PUR are primarily employed in thermal and acoustic insulation and in the automotive sector, owing to their high closed-cell content, low thermal conductivity, high strength-to-weight ratio, and good shock absorption [7].

Polyurethane foam wastes belong to the so-called white pollution [8], and they are mainly destined to landfilling and incineration. Landfilling is the predominant disposal route for polyurethane waste, but the low density of foams results in high landfill space consumption [9,10]. As reported by Kemona et al. [9], air trapped within foam cells can sustain deep-seated fires and hinder extinguishment, while combustion releases highly toxic fumes. In incineration, polyurethane foams are burned to recover energy in the form of heat. Through burning, the volume of waste can be reduced by 99 % [10]. Incineration not only causes the emission of toxic substances and air pollution, but from a circular economic perspective, it causes a significant loss of resources. Mechanical and chemical recycling represent promising alternatives to landfilling and incineration; however, they have not yet become predominant routes for PUFs waste management due to several technical and economic limitations discussed below.

Mechanical recycling is characterized by low cost and simplicity of implementation and consists in reducing the size of the wastes to subject them to further processing, e.g., mixing with adhesives or compression molding. The disadvantages of this type of recycling are related to obtaining cheap products with reduced performance and a limited market [11].

In chemical recycling, functional groups such as urethane, ester, ether, and amine bond can be gradually depolymerized using organic solvent and heat. The main processes used for PUFs include glycolysis, hydrolysis, aminolysis, and phosphorolysis [11]. Considering costs, applied temperature and additional substrates, chemical recycling is still much more challenging than the mechanical one [9].

In recent years, the thermochemical recycling processes of PUFs have attracted great interest because they enable the treatment of not segregate waste streams and allow the decomposition of long polymeric chains into less complex molecules to recover chemical products, energy, and fuels [12]. The main thermochemical processes include pyrolysis, gasification, hydrogenation and hydrothermal methods such as hydrothermal liquefaction (HTL), carbonization (HTC) and gasification (HTG). Hydrothermal processing involves the use of hot-compressed water as reaction medium [13]. The critical point of water is localized at $T_c = 373$ °C and $P_c = 221$ bar [14],. At standard conditions (25 °C and 0.1 MPa), water has a high dielectric constant of 78, making it a polar solvent and generally unsuitable for dissolving nonpolar organic compounds. With increasing temperature, the dielectric constant decreases, reaching a value of 14 at 350 °C. Water at near critical point can dissolve hydrophobic compounds such as polycyclic aromatic hydrocarbons (PAHs) and polychlorinated biphenyls (PCBs) [15].

At 180–280 °C, the hydrothermal process is called HTC, producing a solid carbonaceous residue known as hydrochar (HC). Between 280 and 375 °C, the process is called HTL, yielding a water-insoluble organic liquid (crude), an aqueous phase rich in soluble substances [16].HTC and HTL are promising routes for chemical recycling of polyurethanes, enabling efficient depolymerisation of crosslinked PU using water as a reactive solvent under subcritical or near-critical conditions. Moreover, they do not need energy-intensive pretreatments such as drying, enhancing process sustainability [17]. Owing to these advantages, hydrothermal treatments represent a promising and scalable route for PUR recycling, which forms the focus of the present study.

There are several studies in literature on HTC or HTL processes of waste polyurethanes. Most of them focus on the characterization of the reaction products [18–21] or their potential industrial applications [22–24]. For example, Passos JSd et al. [18] carried out a subcritical hydrothermal liquefaction screening of different plastic including polyurethane foam, working at 350 °C for 20 min. They obtained oil phase with a complex composition containing similar molecules to polyurethane's monomers and longer hydrocarbons. Hartmann D. et al. [19], studied the HTL reactions of TPU working at 250, 300, 350, 400, 450 °C for 60 min. The oil produced at 400 °C was found to have the highest carbon content (70 ± 4 wt%), a calorific value of 33 ± 2 MJ/kg, and a concentration of aniline and *p*-aminotoluene respectively of 94 ± 11 mg/g and 41 ± 3 mg/g.

Other studies have examined the potential uses of solid carbon residues for industrial application.

Chen et al. [22] carried out HTC on PU foam waste from insulating layers of spent refrigerators working at 160–220 ℃ for 2–15 h. The obtained HCs were activated with K_2CO_3 at 800 °C and effectively tested for H_2S adsorption capacity. Duan et al. [23] instead enhances PUFs from dumped sofas working with glutaric dialdehyde (50 %) at 200 °C for 10 h. The solid product was chemically activated using $ZnCl_2$ and the so-prepared nitrogen-doped carbon nanosheets were successfully used for the removal of Cr(VI) from polluted waters. Liu et al., [24] evaluated the use of hydrochar obtained from HTC of PUF with the assistance of glucose, for the use as supercapacitors. The effects on the electrochemical performances were systematically examined in a symmetric two-electrode configuration.Although these studies characterize HTC and HTL products in depth and evaluate their possible applications, none of them addresses in detail how the operating conditions used in the HTC and HTL processes influence the chemical and physical properties of the solid residue. To the best of our knowledge, previous studies investigating the influence of operating parameters in HTC and HTL processes have been conducted exclusively on biomass feedstocks, while systematic analyses for plastic materials are still lacking. In this study, we evaluated for the first time in literature, how the operating conditions employed in the HTC and HTL processes affect not only the reaction yield but also the chemical and physical properties of the resulting solid fractions.

Moreover, the combustion behaviour of the HCs and their possible use as solid fuels were evaluated via TGA-DTG method. For completeness, the liquid phases obtained for each test were analysed by pH measurements and GC-MS analysis.

2. Materials and methods

2.1. Feedstock

A PUR for model making and thoroughly characterized in our

previous study [25] was used as feedstock for the tests. Further characterizations of the foam were carried out in this study using optical and electron microscopy, porosimetry, along with ultimate and proximate analyses. The presence of additives in PUR formulation was evaluated by Soxhlet extraction with acetone. The results of the analysis are reported in paragraph 3.1. Before undergoing hydrothermal processes, the feedstock was cut into small pieces with a long side of approximately one centimeter (Fig. S1).

2.2. Experimental equipment and procedure for HTC/HTL experiments

The HTC/HTL experiments were carried out in a 250 mL alloy 600 Parr autoclave 4576 HP. The heating system consisted of a high wattage ceramic fiber heater. The autoclave was equipped with a stirrer, a pressure sensor (Parr Model 4848) and a J-type thermocouple.

Overall, tests were carried out in duplicate. The operating parameters of each test (temperature, T; reaction time, t_r; feedstock to solvent ratio, f/s) are reported in Table 1. The tests in acidic environment were carried out using a smaller quantity of solution to compare the obtained results with those present in the literature for basic catalysis [25].

The processes scheme is reported in Fig. 1.

For each test a defined quantity of PUR was inserted into the reactor with a specific amount of demineralised water (see Table 1). In tests 5 and 6, an acetic acid solution with pH= 2.0 was used instead of water. The reactor was sealed and before each experiment three purging cycles with Ar (5 bar) were carried out to ensure an inert atmosphere. Finally, the autoclave was loaded with 10 bar of Ar for the test. The reaction time was measured only after reaching the target temperature. The time required to reach 250 °C was approximately 30 min, whereas about 56 min were required to reach 345 °C. The heating rates for each temperature are reported in Figure S2 in the Supplementary Information. All the tests were carried out without stirring. Although the absence of agitation in hydrothermal reactions can limit heat and mass transfer, potentially reducing product yields and reaction uniformity [26], in this study mechanical stirring was not feasible due to the bulky nature of the plastic feedstock which occupied the entire body of the reactor (Fig. S3) preventing the movement of the stirrer and damaging the stirrer shaft.

At the end of the reaction, the autoclave was cooled at room temperature, and the gas was vented out. The slurry was filtered under vacuum, and the liquid phase is separated from the wet cake. The wet cake was washed several times with acetone and then dried in a oven at 50 °C until constant weight. The solid product thus obtained was the HC. The obtained HCs were characterized by elemental analysis, FTIR spectroscopy, SEM analysis and their combustion properties were evaluated by TGA-DTG. A qualitative analysis of the organic compounds in liquid phase was carried out at the end of each test. The liquid phase (LP) consisting of the process water and chemicals was subjected to a liquid-liquid extraction. In particular, 20 mL of the liquid phase were placed in a separating funnel together with 20 mL of dichloromethane (DCM). Once the two fractions have been separated, the residual moisture in the DCM fraction was removed using anhydrous sodium sulphate. Then the two fractions were dried under nitrogen flow and subsequently injected into GC-MS using methanol as solvent. The aqueous fraction is designated AP, while the organic fraction is designated OP. This procedure was adopted for all samples except for ID5 and ID6, to minimize their handling due to potential safety concerns related to the possible formation of hydrogen cyanide in the acidic reaction conditions. We are aware that the absence of a liquid-liquid extraction can lead to certain analytical disadvantages such as lower selectivity, lower sensitivity and matrix effects.

2.3. Determination of the solid residue yield

From each HTC/HTL experiment the yields of the solid fraction were calculated using Eq. 1, in which w_{solid} indicates the weight of the solid product recovered from the reaction and $w_{feedstock}$ indicates the weight of the feedstock used in the test.

$$Solid\ residue\ yield(\%) = \frac{w_{solid}}{w_{feedstock}} * 100 \quad (1)$$

2.4. Analytical methods

2.4.1. Extraction of PUR additives in Soxhlet

Additives extraction was carried out in a Soxhlet [27] for 8 h using 100 mL of acetone, 177.9 mg of foam and at 84 °C. At the end of the reaction, the solvent was evaporated from the flask using a N_2 flow, and the additives were solubilized in methanol for subsequent injection into GC-MS.

2.4.2. Analysis of liquid phase

2.4.2.1. pH measurement. pH measurements were carried out using the pH60 Violab equipped with XS 201 T DHS digital electrode with integrated temperature sensor. Before each measurement the pHmeter was calibrated with standard solutions at pH 4 and 7.

2.4.2.2. GC-MS. The analyses were performed with a GCMS-QP2020 NX instrument (Shimadzu, Nishinokyo Kuwabara-cho, Kyoto, JP), equipped with a SH-Rxi-5 ms column (length 30 m, internal diameter 0.25 mm, film diameter 0.25 μm). The injector temperature was set at 280 °C, while a gradient from 55 to 300 °C was set for the column over a total of 25 min (heating rate: 9.8 °C/min). Qualitative analysis was performed by comparing the mass spectra with those of the NIST 20 library. Only compounds with a match greater than 85 % were considered, the others were designated "unknown".

2.4.3. Analysis of feedstock and solid phase

2.4.3.1. Digital microscopy. Images of the foam structure were acquired using the digital microscope Andonstar AD249S-M equipped with the lens D, with magnification ratio of 1800–2040x. The device features an adjustable stand, integrated LED illumination, and real-time image capture capability via HDMI or USB connection, allowing for precise visualization and documentation of surface morphology.

2.4.3.2. Scanning electron microscopy. SEM micrographs were acquired using a Zeiss Sigma FE-SEM equipped with a GEMINI column and In-

Table 1
Operating parameters for each test.

ID	T (°C)	t_r (min)	Feedstock (g)	Solvent (mL)	f/s	Catalyst	ID abbreviation
1	250	120	3	150	0.02	-	ID1 $_{250\_120\_0.02}$
2	250	120	3	100	0.03	-	ID2 $_{250\_120\_0.03}$
3	250	20	3	100	0.03	-	ID3 $_{250\_20\_0.03}$
4	345	20	3	100	0.03	-	ID4 $_{345\_20\_0.03}$
5	250	120	3	70 (pH=2.0)	0.04	Acetic acid	ID5 $_{250\_120\_Ac}$
6	345	20	3	70 (pH=2.0)	0.04	Acetic acid	ID6 $_{345\_20\_Ac}$
7	250	120	6	100	0.06	-	ID7 $_{250\_120\_0.06}$
8	345	120	3	100	0.03	-	ID8 $_{345\_120\_0.03}$

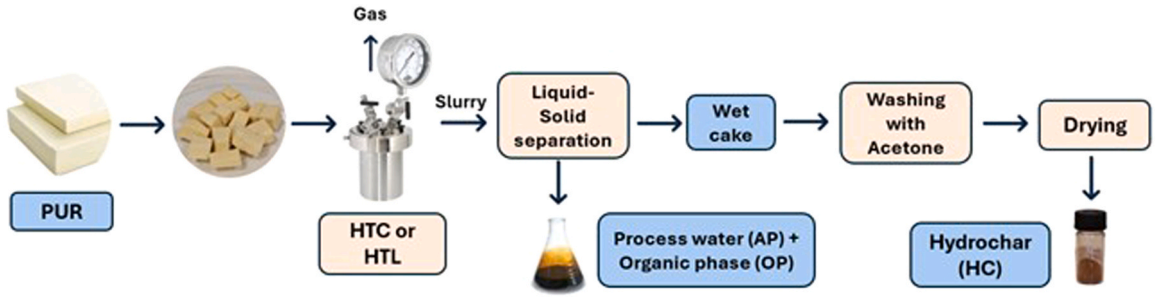

Fig. 1. Processes scheme for HTL and HTC.

Lens detector, capable of providing high-resolution images on conductive and non-conductive samples. The microscope was operated at low voltage of 2 kV, working at a distance of about 3 mm with magnification of 20000. The microscope is also equipped with an X-ray detector (EDS) and a backscattered electron (BSE) and secondary electron (SE) detector.

2.4.3.3. Porosimetry. Mercury intrusion porosimetry was carried out using a Micromeritics AutoPore V porosimeter equipped with a 5-bulb penetrometer to determine the pore size distribution, total pore volume, pore surface area, porosity, and densities of the sample. The analysis was performed in two stages: a low-pressure (LP) run and a high-pressure (HP) run. The instrument operated over a pressure range from 0.10 psia to 61,000.00 psia, enabling the detection of pore diameters ranging from approximately 3 nm to several microns, based on the Washburn equation, assuming a contact angle of 140° and a mercury surface tension of 485 dyn/cm. Prior to analysis, PUR sample was degassed and dried at 105 °C to remove moisture.

The PUR sample used had a mass of 0.0308 g and was loaded into a penetrometer with a volume of 5.8752 mL and a mass of 63.5332 g. The mercury temperature during the measurement was 26.01 °C, and a blank correction was applied. A stem volume usage of 68 % was recorded. Both bulk density and skeletal density were measured, and the total porosity was calculated from these values.

2.4.3.4. FTIR spectroscopy. FTIR spectra of the samples were obtained using a Shimadzu IR Tracer-100 spectrometer, equipped with a QATR 10 Single-Reflection ATR with a Diamond Crystal (Shimadzu, Nishinokyo Kuwabara-cho, Kyoto, JP), operating with a maximum resolution of 0.25 cm^{-1} and a spectral range in the mid-IR region (4100–500 cm^{-1}). The spectra have been acquired in transmittance mode (%) using 45 scans for each sample.

2.4.3.5. Ultimate analysis. The ultimate analysis was carried out using the Flash Smart Elemental Analyzer CHNS/O instrument (Thermoscientific, Waltham, Massachusetts, USA). The instrument allows the quantitative determination, fully automated, of the elements C, H, N, S and O by chromatographic analysis of combustion gases. The gases, formed during the combustion process, are detected by a thermal conductivity detector (TCD). A calibration curve with standard compounds (acetanilide, sulfanilamide or 2,5-bis(5-tert-butyl-2-benzo-oxazol-2-yl) thiophene was carried out before each session analyses. Measurements were carried out in duplicate for each sample and the percentage of oxygen was calculated by difference.

2.4.3.6. Proximate analysis. The proximate analysis was carried out in accordance with the standard UNI EN 15414–3:2011, UNE 32–004–84, UNE-EN 15402.

2.4.3.7. Calculation of higher heating value (HHV). According to Kalivodova et al. [28] the HHV is defined as the amount of heat that is released by the perfect combustion of the fuel sample and the subsequent cooling of the flue gases to the original temperature, while the water released by combustion condenses and the energy of the chemical re-action does not need to be reduced by its latent heat. In this study the HHV value of the PUR and HCs was calculated by Boie's equation [28, 29] reported below (Eq. 2) using the elemental analysis data.

$$HHV = 351.7C + 1162.6H - 110.9O + 104.7S \quad (2)$$

C, H, O, N and S are on a % dry weight basis.

As explained by Glova et al. [29] the oxygen term has negative coefficients, because it ties up some of the carbon and hydrogen in the form of CO, H_2O and phenols (OH).

2.4.3.8. Thermogravimetric analysis. The thermogravimetric analysis of the sample was carried out with an SDT 650 instrument (TA Instruments, USA). Each time about 10.00 mg of sample were placed into an alumina crucible. Measurements were performed in the temperature range 25–900 °C with a heating rate of 10 °C/min and an air flow rate = 100 mL/min. Using the TG-DTG curves, the basic combustion parameters were determined, i.e. the ignition temperature T_i (°C), the peak temperature T_p (°C) and the final temperature T_f (°C) [30]. These parameters reflect the thermal behavior of the samples during the combustion process [31]. T_i is defined as the temperature at which a sample starts burning and is determined by the TG-DTG tangent method [32]. T_f corresponds to where the weight becomes constant at the completion of burning and the DTG profile reaches a 1 wt% per minute combustion rate at the tail-end of the profile [33]. The peak temperature is defined as the temperature corresponding to the peak of the DTG profile [34].

The ignition index (D_i) is expressed by Eq. 3:

$$D_i = \frac{DTG_{max}}{t_p \cdot t_i} \bullet 100 \quad (3)$$

where DTG_{max} is the maximum combustion rates, t_p is the corresponding time of DTG_{max}, t_i is the ignition time. D_i represent the ignition performance of fuels, which reflects how difficult or easy and how fast and slow the fuel gets ignited [33].

3. Results and discussion

3.1. Feedstock characterization

According to the data obtained from the ^{13}C NMR analysis, carried out in our previous study [25] the polyurethane rigid foam used for this study contains a hard segment made up of an aromatic isocyanate, the methylene diphenyl diisocyanate (MDI) and a chain extender, the 2-methyl-1,3-propanediol (MPD). The soft segment composition was deduced from the chemical species identified through GC-MS analysis of the liquid fractions collected during the experiments conducted at 250 °C. The identified chemicals, such as propylene glycol and 1–1′-oxybis-2-propanol, suggest that the soft segment of the foam can be a polypropylene glycol triol type as shown in Figure S4. According to literature [35,36], these types of polyols are used to form highly cross-linked polyurethanes, such as rigid foams.

Soxhlet extraction of PUR with acetone provided information on

some additives used in the formulation. The results of GCMS analysis on the extract are reported in Table S1.

The extraction highlighted the presence of N,N-dimethylcyclohexylamine (DMCHA), a typical tertiary amine used as a catalyst in the synthesis of rigid polyurethane foams as described in literature [37,38] and in numerous patents [40]. The PUR foam also contains tris(1-chloro-2-propyl) phosphate (TCPP), a chlorinated organophosphate ester mainly used as flame retardant [41]. Based on the recent toxicity studies, TCPP may impact nervous system development as well as thyroid hormone levels [42]. Finally, the extraction highlighted the presence of some phthalates generally used as plasticizers (diisobutyl phthalate, DIPB and dibutyl phthalate, DBP). Phthalates are typically used in polyurethane flexible foam to improve elasticity, compression, and recovery properties but in agreement with literature, phthalates can be also used in rigid foam. According to Wadey [43], small additions of 2–5 phr (parts per hundred rubber) of benzyl butyl phthalate (BBP) in rigid foams leads to higher compressive strength, finer cell structure and stronger cell wall than non-plasticized polymer. The resulting foam is stronger, insulates better and is durable to environmental degradation.

The ultimate analysis, proximate analysis and HHV value for PUR are reported in Table 2. The obtained data are comparable with those presented in literature for similar systems [44–46].

PUR was also characterized by digital and electron microscopy. The image of PUR under the digital microscope in Fig. 2a reveals a macrocellular polymeric foam with cell dimensions larger than 100 μm [6].

The walls, struts and nodes are clearly visible. As described by Beverte et al., [47] a wall is a polymeric interface between two bubbles; a strut is a polymeric element, formed by the flow of the liquid reacting mixture through Gibbs channels formed by the contact of three bubbles; a node is an un-foamed polymeric volume entered by ~4–6 struts.

The SEM micrograph in Fig. 2b confirms the complex cell structure with walls (cell faces) and struts formed at the cell junction. The walls are thinner than the struts and the cell diameter is much larger than the strut thickness [48].

Mercury intrusion porosimetry revealed that the material exhibits a high total intrusion volume of 8.47 mL/g, corresponding to a substantial pore space. The calculated porosity was 89.5 %, indicating a highly porous structure. The bulk density, measured at low pressure (0.49 psia), was 0.11 g/mL, while the skeletal density at high pressure (60,987.99 psia) was 1.01 g/mL, confirming the lightweight and porous nature of the sample. The total pore surface area was found to be 54.0 m^2/g. Pore size analysis showed a volume-based median pore diameter of 2.690 nm, suggesting that macropores dominate the overall pore volume. In contrast, the area-based median pore diameter was 3.86 nm, indicating that the surface area is largely contributed by finer pores. The average pore diameter, calculated as 4 V/A, was 628 nm, supporting the coexistence of a wide pore size distribution within the material.

3.2. HCs yields

The HCs yields for each test are reported in Fig. 3. A first consideration of the obtained results can be assessed by examining the effect of temperature and reaction time.

In agreement with what has been described in literature for biomass and plastic materials, also for PUR temperature seems to be the governing parameter for hydrothermal processes [16, 49–51].

A drastic increase in temperature from 250 °C (ID2 $_{250\_120\_0.03}$) to 345 °C (ID8 $_{345\_120\_0.03}$), while keeping other operating parameters unchanged, caused a drastic decrease in HC yield from 19.5 % to 1.8 %. We can explain this result by considering that an increase in temperature provides energy in the form of heat [16], which causes a degradation of the macromolecules in the feedstock, favouring the formation of the liquid fraction.

During the study, the effect of two different residence time (20 min and 120 min) was also evaluated, working both at 250 °C (ID2 $_{250\_120\_0.03}$ and ID3 $_{250\_20\_0.03}$) and 345 °C (ID4 $_{345\_20\_0.03}$ and ID8 $_{345\_120\_0.03}$). According to biomass literature there is a debate on the effect of residence time on hydrothermal processes. As reported by some studies [52,53] longer residence times would favor the solid residue production due to the repolymerization of the species in solution, with formation of secondary hydrochar. Instead for other studies [54] the influence of residence time is not significant on HC yields.

In the case of PUR, at 250 °C the increase in reaction time leads to an increase in HC yield (from 7.7 % of ID3 $_{250\_20\_0.03}$ to 19.5 % of ID2 $_{250\_120\_0.03}$).

Conversely, at 345°C the increase in reaction time leads to a decrease in HC yield (from 12.5 % of ID4 $_{345\_20\_0.03}$ to 1.8 % of ID8 $_{345\_120\_0.03}$). Once again, temperature appears to play a decisive role in reaction yield.

The combined effect of temperature and residence time can be described by a single parameter, called severity factor, reported in Eq. 4:

$$R_0 = t \bullet \exp\left(\frac{T-100}{14.75}\right) \quad (4)$$

where t, is the residence time (min); T, the temperature (°C); 100, a reference temperature below which the reaction is negligible; 14.75 is the activation energy (kJ/mol) based on the assumptions that the reaction is hydrolytic and the overall conversion is first-order [55]. The value of log(R_0) is usually reported, and this will be referred to as "severity value" (SV) [56]. The SVs of each test are reported in Table S2 and the 3D plot HC yields vs SV vs time is reported in Fig. 4.

The SVs show an inverse relationship with hydrochar yield: as severity increases, the solid residue tends to decrease, confirming the expected HTL behavior. In particular, the extremely low yield observed for ID8 $_{345\_120\_0.03}$ (SV= 9.3) suggests extensive feedstock degradation and carbon loss. The lowest SV, 5.7, is related to ID3 $_{250\_20\_0.03}$. For low severity values, efficient depolymerisation of PUR is observed (Figure S5) but the mild reaction conditions do not favour the formation of HCs.

The highest HCs yields were obtained for tests ID1 $_{250\_120\_0.02,}$ ID2 $_{250\_120\_0.03,}$ ID7 $_{250\_120\_0.06}$, carried out with SV= 6.5 in absence of acid catalyst. These tests were conducted working at the same temperature (250°C) and residence time (120 min) but with different f/s ratio, 0.02, 0.03, 0.06 respectively. The obtained results suggest that an increase in f/s ratio does not lead to a significant increase in HC yield. The relationship between f/s and HC yield does not find consensus in the HTC literature. According to some studies on biomass, such as that of Volpe and Fiori [57] (f/s values=0.07/0.10/0.15/0.25) an increase in the f/s causes an increase in HC yield; instead for other work such as that of Tag et al., [58] (f/s in the range between 0.05 and 0.55) the effect of solid

Table 2
Ultimate analysis, proximate analysis and HHV value for PUR.

	Ultimate Analysis[a] (wt%)				Proximate analysis (wt%)				HHV (MJ/kg)
Sample	C	H	O[b]	N	Moisture	Volatiles	Fixed Carbon[c]	Ashes	
PUR	63.96 ± 0.13	6.34 ± 0.06	23.69 ± 0.11	5.78 ± 0.03	1.28 ± 0.02	80.11 ± 0.20	18.38 ± 0.20	0.23 ± 0.04	27.60 ± 0.19

[a] On a dry basis
[b] By the difference: O%= 100 - (C%-H%-N%- Ashes)
[c] By the difference: FC= 100 - moisture – volatiles - ashes

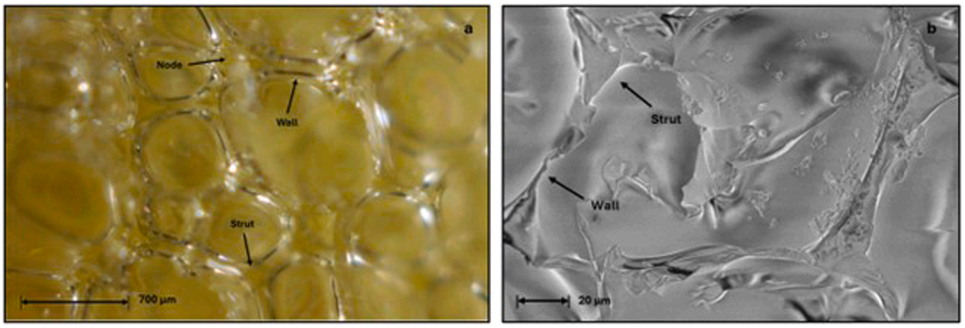

Fig. 2. Structure of PUR under digital microscope (a); SEM micrograph of PUR (b).

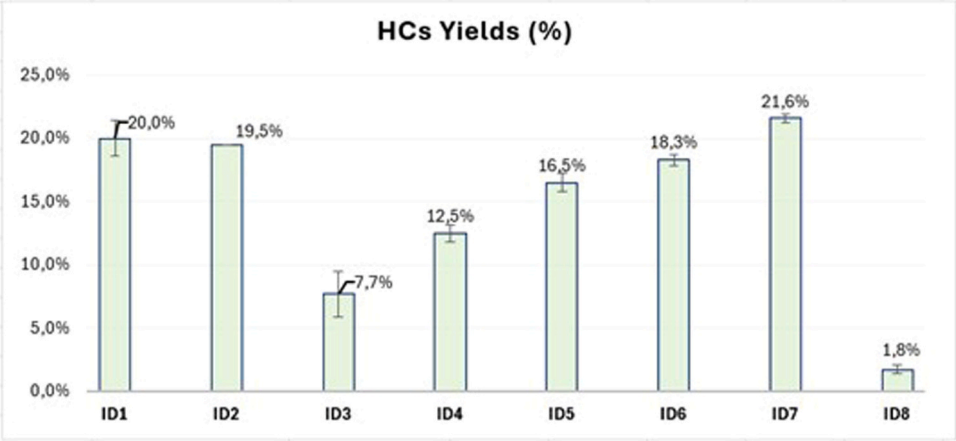

Fig. 3. Yields in HCs formation in all the investigated processing conditions.

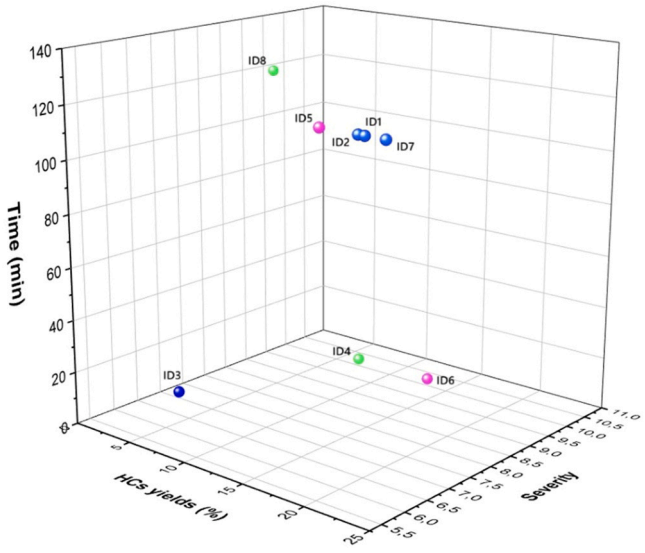

Fig. 4. HC yields vs SV vs time for each test.

load was found insignificant.

In this study, higher f/s values could not be investigated, once again due to limitations connected with the bulky nature of the plastic feedstock.

The yields for ID5 $_{250\_120\_Ac}$ (SV= 6.5) and ID6 $_{345\_20\_Ac}$ (SV= 8.5) are respectively 16.5 % and 18.3 %. Although the severity values are the same as those used in previous tests, different yield values are observed. This variability can be explained by the effect of the acidic reaction environment. In particular, when comparing the data obtained with those reported in the literature at similar SV but for basic environments no significant reduction in HC yield is observed. According to the study of Gallorini et al. in HTL test carried out with SV= 8.7 and in presence of KOH as catalyst, the HCs yield drops to 1 % [25]. Also according to Wang et al. bases are more effective than acid for the HTL of PU [20].

3.3. pH analysis of liquid phases

The pH values of liquid phases (LPs) for each test are shown in Table S3.

The LPs of tests ID1, ID2, ID3, ID4, ID7 and ID8 show acidic pH value close to or below 5. Since GCMS analysis did not reveal the presence of organic acids in solution, this pH value could be justified by the release of HCl from the chlorinated flame retardant (TCCP) used in foam formulation. This phenomenon of pH lowering after hydrothermal treatment has been described in the literature for plastics feedstock containing organic bromine compounds, due to the release of HBr in the solution [30].

The acetic acid solutions used in ID5 and ID6 had an initial pH value of 2.0. At the end of the tests the liquid phase showed a pH of 2.9 for ID5 and 3.0 for ID6, respectively. This little increase in pH value is not only due to the formation of basic compounds such as anilines and quinolines, but also to a partial reaction of the acetic acid in the reaction environment, forming esters and amides, as described in paragraph 3.4.

3.4. GC-MS analysis of liquid phases

The liquid phases of the tests carried out at 250 °C are rich in organic compounds. As shown by Fig. 5a, the AP of ID1 $_{250\_120\_0.02}$ contains propylene glycol, 2-propanol-1,1′-oxybis, dipropylene glycol. These

chemicals are derived from the depolymerization of the soft segment of polyurethane and are commonly identified in literature [22]. Also fragments from the depolymerization of rigid segment are visible as aniline (both in AP and OP), variously substituted benzamines and condensation compounds such as quinolines (OP, Fig. 5b). The formation of aniline during an HTL process of polyurethanes is described in the work of Hartmann et al. [19]. Polyurethane dissociation occurs via −NH transfer and subsequent hydrolysis of the formed diisocyanate. Hydrolysis of MDI occurs spontaneously during HTL because of the high temperature and pressure, and it is converted to carbamic acid and subsequently to a primary amine and CO_2.

Working at the same temperature (250 °C) but under more concentrated conditions (f/s = 0.06, ID7 $_{250\_120\_0.06}$), aniline is still present in AP while the OP shows a higher content of benzamines and condensation compounds such as quinolines (Fig. 5b). Probably this result is due to the smaller amount of water then feedstock which favors the recombination of monomers in solution.

Figure S6 shows the percentage areas of the compounds identified in the AP and OP for the test ID8 $_{345\_120\_0.03}$. In this case, the high temperatures seem to reduce the number of compounds present in solution by favoring almost exclusively the formation of variously substituted quinolines. Quinolines are widely used in the production of synthetic dyes and have a high industrial value [59].

The liquid phases of ID5 $_{250\_120\_Ac}$ and ID6 $_{345\_20\_Ac}$ were dried under nitrogen flow and solubilized in MeOH without a previous liquid-liquid extraction as explained in paragraph *2.2*.

The LPs resulted rich in organic compounds and this suggests that the acidic environment catalyzes the liquefaction reactions, favoring the formation of low molecular weight compounds visible by GCMS. Both LPs shown compounds resulting from the condensation reaction of acetic acid with polyols and amines as 1,2-ethandiol monoacetate, 2-(2-hydroxyethoxy)ethyl acetate, N-phenyl acetamide, N-(2-methylphenyl) acetamide, N-(4-methylphenyl) acetamide. The formation of these compounds explains the increase in pH observed for ID5 and ID6 compared to the initial value of acetic acid solution.

Moreover, the LP of ID6 $_{345\_20\_Ac}$ showed aromatic heterocyclic compounds as isoquinoline, 3-methyl isoquinoline, 2,4-dimethyl-quinoline, 1,4-dihydro-1,2-dimethylquinolin-4-ylidenemethane. Once again we can observe how the increase in temperature favors the formation of aromatic heterocyclic compounds.

3.5. Solid residues analysis

3.5.1. FTIR spectra

Fig. 6 shows the FTIR spectra of the obtained HCs. To facilitate comparison, the spectra were grouped by temperature: tests at 250°C (6a); tests at 350°C (6b) and tests in presence of acidic catalyst (6c). Each set of spectra was compared with the FTIR of the original foam (black line).

HCs from ID1 $_{250\_120\_0.02}$, ID2 $_{250\_120\_0.03}$, ID3 $_{250\_20\_0.03}$, ID7 $_{250\_120\_0.06}$ showed similar absorptions with each other and with the feedstock (Fig. 6a). N-H stretching at around 3358 cm^{-1}, C-H stretching of aromatics (3000 cm^{-1}) and aliphatics (2962–2894 cm^{-1}) are evident for all the examined samples. In HCs, an absorption at 3441 cm^{-1} is also visible, which can be assigned to the N-H of pyrrole groups. This result is consistent with the results emerging from the ultimate analysis reported in Section 3.5.2.

PUR showed also the characteristic absorption at 2300 cm^{-1} related to the presence of unreacted isocyanate groups. A slight shift of the C═O stretching is observed from 1744 cm^{-1} (stretching of esters) of PUR to approximately 1715 cm^{-1} (stretching of aliphatic ketone) in HCs. The peak related to this absorption in HCs is less intense than that in the feedstock. In contrast, the C-O stretching band (1100–1045 cm^{-1}) of PUR disappeared in the HCs. These data agree with the oxygen percentage reduction observed by elemental analysis (paragraph 3.5.2) and confirm that decarboxylation reactions are important phenomena during the hydrothermal process. The similarity of FTIR spectra among HCs produced at 250 °C indicates that, under these conditions hydrochars still retain several functional features of the original polymer, and dehydration reactions are already active but remain limited in extent at this temperature.

Fig. 6b shows the FTIR spectra of HCs from ID4 $_{345\_20\_0.03}$ and ID8 $_{345\_120\_0.03}$, both obtained at 345 °C but for different reaction times (20 and 120 min respectively). Signals related to N-H stretching disappear in comparison to PUR while those of C-H stretching remain faintly visible. In HC from ID4, the absorption at 1738 cm^{-1} relative to C═O is still visible. Both the HCs samples show a small band at about 1601 cm^{-1} related to the aromatic C═C stretching. The presence of aromatic C═C stretching bands indicates that condensation and aromatization reactions become significant at this temperature, even at short reaction times as in ID4.

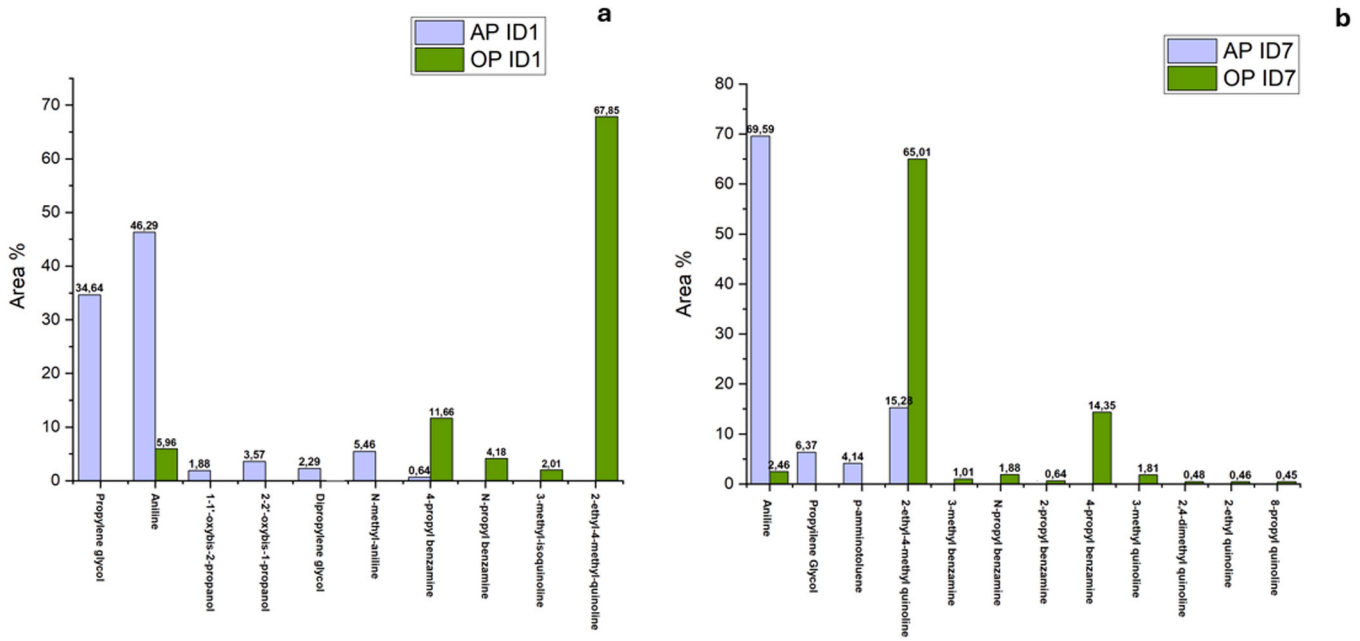

Fig. 5. Percentage areas of the compounds in the AP and in the OP of ID1 (a) and ID7 (b).

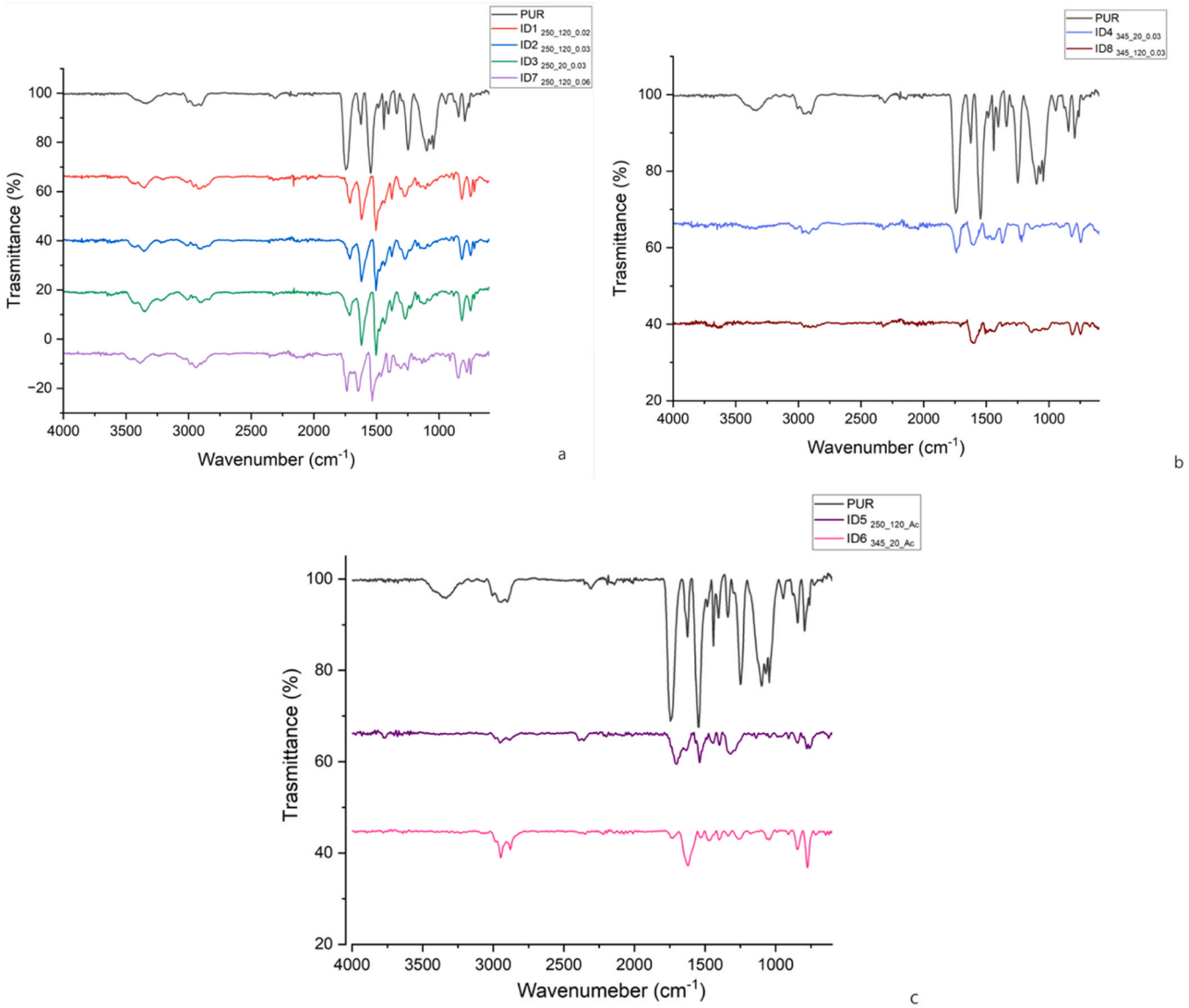

Fig. 6. FTIR spectra of the obtained HCs grouped by processing conditions: 250 °C (Test ID1, ID2, ID3, ID7) (6a), 350 °C (Test ID4, ID8) (6b), and acidic-catalyst tests (6c). The spectrum of the original foam (black line) is shown for comparison.

Fig. 6c shows the FTIR spectra of HCs from ID5 $_{250\_120\_Ac}$ and ID6 $_{345\_20\_Ac}$. In both samples, the N-H stretching signals disappear. The disappearance of N–H stretching bands in acid-treated hydrochars can be rationalized considering the simultaneous formation of nitrogen-containing compounds detected in the corresponding liquid phases (paragraph 3.4). In ID5 the C═O stretching shifts from 1744 cm^{-1} to 1690 cm^{-1}. This value is characteristic of C═O stretching of tertiary or cyclic amides. In ID6 the C═O stretching at 1731 cm^{-1} is very weak but still present. In both HCs spectra, the absorptions related to C═C aromatic stretching are clearly visible at 1535 cm^{-1} (ID5) and at 1610 cm^{-1} (ID6).

3.5.2. *Ultimate analysis*

The ultimate analysis of PUR and HCs are shown in Table 3.

Elemental analysis of the HCs reveals a substantial increase in carbon content (up to 78.7 %) compared to the feedstock (63.96 %), together with a pronounced reduction in oxygen content (from an initial 23.69 % to values ranging between 6.12 % and 13.64 %). At the same time, an increase in nitrogen content is observed, reaching values up to 10.70 %, compared to 5.78 % for the original PUR. The low atomic H/C ratio (from 0.10 to 0.07–0.08) and the reduction of the O/C ratio (from 0.37 to 0.08–0.19) suggest aromatisation and deoxygenation of the solid residues. In particular, the increase in carbon content and the reduction in O/C can be attributed to carbonisation, decarboxylation and dehydration reactions, which result in the selective loss of oxygenated groups in the form of CO_2 and H_2O [60]. The increase in the percentage of nitrogen in HCs suggests the formation of stable nitrogenous aromatic structures and it has already been described in literature [22,23], in which the HCs appears a promising feedstock to produce nitrogen-doped carbon materials. Nitrogen-rich HCs can be successfully exploited after a chemical activation for the removal of water contaminants such as Cr (VI) and H_2S.

The Van Krevelen diagram showed in Fig. 7 was used to present the fuel properties of derived HCs by plotting hydrogen/carbon (H/C) ratios against oxygen/carbon (O/C) ratios. This type of diagram allows to identify the reaction processes which involve the feedstock: oxidation/reduction reactions appear as a shift in the O/C ratio; hydrogenation/dehydrogenation reactions appear as a shift in the H/C ratio; methylation/demethylation and hydrolysis/ condensation reactions appear as shifts in both H/C and O/C ratios on a diagonal [61].

PUR has H/C ratio and O/C ratio of 0.10 and 0.37 respectively and fall into the peat region, which is characteristic of highly oxygenated

Table 3
Ultimate analysis of PUR and HCs.

ID	C (%)	H (%)	N (%)	O (%)	S (%)	H/C	O/C
PUR	63.96 ± 0.13	6.34 ± 0.06	5.78 ± 0.03	23.69 ± 0.11	-	0.10 ± 0.00	0.37 ± 0.00
ID1250_120_0.02	78.23 ± 1.44	5.56 ± 0.79	9.53 ± 0.28	6.40 ± 0.55	-	0.07 ± 0.01	0.08 ± 0.01
ID2 250_120_0.03	78.33 ± 1.07	5.86 ± 0.03	9.69 ± 0.07	6.12 ± 1.03	-	0.07 ± 0.00	0.08 ± 0.01
ID3 250_20_0.03	77.02 ± 1.05	6.08 ± 0.02	10.70 ± 0.05	6.20 ± 0.12	-	0.08 ± 0.00	0.08 ± 0.00
ID4 345_20_0.03	78.70 ± 0.66	6.32 ± 0.05	7.56 ± 0.17	7.42 ± 0.35	-	0.08 ± 0.00	0.09 ± 0.00
ID5 250_120_Ac	73.70 ± 0.22	5.97 ± 0.78	6.69 ± 0.25	13.64 ± 0.54	-	0.08 ± 0.01	0.19 ± 0.00
ID6 345_20_Ac	75.58 ± 1.03	5.13 ± 0.61	6.61 ± 0.11	12.68 ± 0.14	-	0.07 ± 0.00	0.17 ± 0.00
ID7 250_120_0.06	77.80 ± 1.45	6.40 ± 0.04	9.10 ± 0.06	6.55 ± 0.45	-	0.08 ± 0.00	0.08 ± 0.00
ID8 345_120_0.03	76.49 ± 1.04	5.22 ± 0.18	7.67 ± 0.07	10.62 ± 0.80	-	0.07 ± 0.00	0.14 ± 0.01

and weakly aromatized organic materials. Instead, all the HCs have H/C and O/C atomic ratios close to the coal region characterized by H/C of 0.6–1.1 and O/C of 0.05–0.30 [62]. There are few studies in the literature regarding the characterization of polyurethane hydrochar as fuel. The comparison of our data with that reported in the work of Islam and Reza [63], indicates that hydrochars produced from polyurethane alone display improved fuel properties compared to those obtained through co-hydrothermal carbonization of polyurethane and biomass as corn stover, as the latter exhibit higher O/C atomic ratios.

According to Sliz and Wilk, a fuel with low H/C and O/C ratios is favourable because of the reduced energy loss, smoke and water vapour during the combustion process [64].

3.5.3. Higher heating value and energy densification ratio of HCs

The HHV values of PUR and HCs, and the Energy Densification Ratio (EDR) are shown in Table 4.

All the HCs show a HHV higher than that of PUR itself (27.59 MJ/kg), and this result is indicative of energy densification process. The EDR values show an increase in the energy content of the solid residues than the raw substrate [65] and they were calculated as ratio between the HHV of HCs on the HHV of PUR, as shown by Eq. 5:

$$EDR = \frac{HHV_{HC}}{HHV_{PUR}} \quad (5)$$

The highest energy densification value is observed for ID4, obtained by working at 345 °C for 20 min.

Fig. 8 shows both the effect of solid loading (f/s) on HCs yields and HHVs. As explained in paragraph 3.2 the increase of f/s ratio does not lead to a significant increase in HC yield showed by the blue histograms,

Table 4
HHV and EDR of PUR and HCs.

ID	HHV (MJ/kg)	EDR
PUR	27.59	-
ID1 $_{250\_120\_0.02}$	33.86	1.23
ID2 $_{250\_120\_0.03}$	34.28	1.24
ID3 $_{250\_20\_0.03}$	34.13	1.24
ID4 $_{345\_20\_0.03}$	34.67	1.26
ID5 $_{250\_120\_Ac}$	31.76	1.15
ID6 $_{345\_20\_Ac}$	31.55	1.14
ID7 $_{250\_120\_0.06}$	34.64	1.25
ID8 $_{345\_120\_0.03}$	32.26	1.17

but causes a slight increase in the HHV of the solid residues, which pass from 33,86 MJ/kg for ID1, to 34.28 for ID2 and 34.64 MJ/kg for ID7. This trend in the HHVs, has been described in the literature for HTC from biomass as sewage sludge [66,67] and anise [68].

The HCs from tests 5 and 6 exhibit the lowest calorific values. This can be justified by the high oxygen content detected by elemental analysis in the solid residues. According to the Boie's equation [28], oxygen has a negative contribution on the calorific value, reducing it.

It is interesting to note that the calorific value of HC from test 8 is lower than that of HC from test 4. This data can again be explained by the higher oxygen content in HC of ID8 compared to HC of ID4 $_{345\_20\_0.03}$. We can assume that for higher temperature and longer reaction times oxygenated compounds present in the liquid phase can condense on the solid phase [69] giving a secondary char rich in oxygenated aromatic compounds.

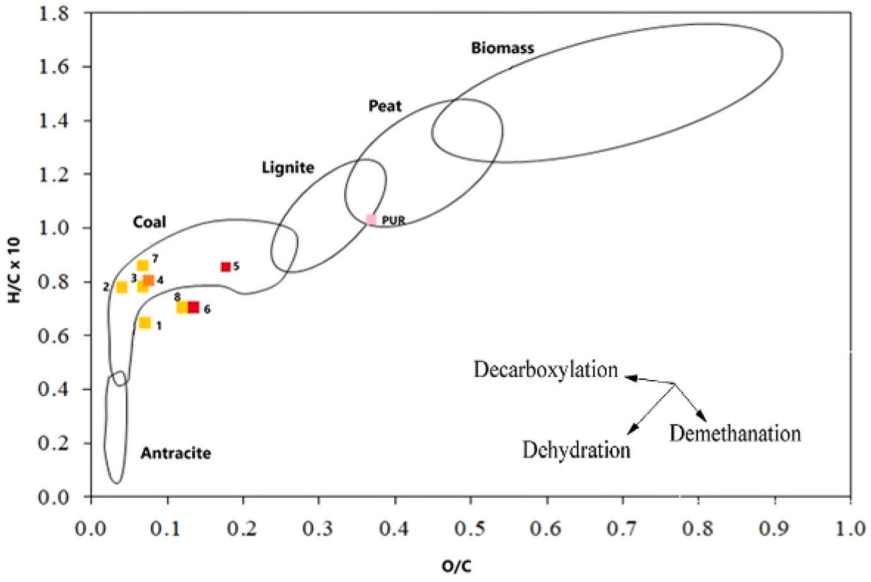

Fig. 7. Van Krevelen's Diagram of PUR and HCs.

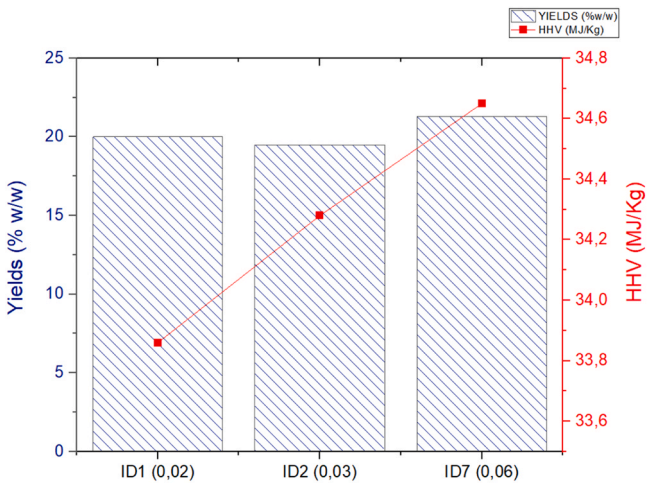

Fig. 8. Effect of solid loading on HCs yields (blue histograms) and HHVs (red trend).

3.5.4. *Morphology features of HCs*

SEM micrographs on HCs are shown in Fig. 9 (magnification 20 kX) and Figure S7 (magnification 5 kX) in Supplementary Information. The analysis revealed a strong morphological dependence on reaction temperature, residence time and presence of catalyst.

For HCs from ID1$_{250_120_0.02}$ and ID2 $_{250\_120\_0.03}$, micrographs show the coexistence of two distinct morphologies. Flat areas alternate with porous areas (i.e. porosity in the order of hundreds of nm: 100–300 nm). These sub-micron porous zones were generated during the hydrothermal process, probably due to the explosion of gas bubble on the surface of PUR. HCs from ID3 $_{250\_20\_0.03}$ and ID4 $_{345\_20\_0.03}$ show smooth, undeveloped surfaces due to the low reaction time (20 min). Cavities in the order of a few micrometers are observed, probably belonging to the unconverted feedstock (Fig. S7). As shown by HCs from ID5 $_{250\_120\_Ac}$ and ID6 $_{345\_20\_Ac}$ micrographs, acidic environment generates surface micro structuring with lamellae's fragments with dimensions in the order of hundreds of nm. The use of acetic acid as a catalyst seems to enhance significantly the breakdown of the polyurethane matrix, as shown by the more fragmented and exfoliated morphology of the HCs and by the results of GCMS. HC from ID7 $_{250\_120\_0.06}$ shows a compact surface that can be justified by the high f/s ratio (i.e. 0.06). According to literature a greater quantity of water (as in ID1 $_{250\_120\_0.02}$ and ID2 $_{250\_120\_0.03}$) guarantees a better heat and mass transfer in the reaction medium favouring phase micro-separation and decomposition of the feedstock, instead higher solid loadings limit solvation and heat transfer. Moreover, HC from ID7 $_{250\_120\_0.06}$ appears to be a poorly conductive sample. This can be explained by the persistence of organic decomposition products on its surface [70] due to the low water content. The HC from ID8 $_{345\_120\_0.03}$ shows an extremely uneven morphology, with mesoporous zones alternating with flat regions, surface cracks and microspheres. The use of high temperatures with sufficient residence time may lead to a high degree of intermediate dissolution products and their subsequent re-polymerization and agglomeration in microspheres, forming secondary char [71], as visible in the SEM micrograph of Fig. S7.

3.5.5. *Solid residues combustion behaviour analysis*

To verify the possible use of the obtained HCs as solid fuels, TG and DTG analysis of PUR and HCs samples were performed under air conditions. For the analysis, only HCs obtained at 250 °C were examined (ID1 $_{250\_120\_0.02}$, ID2 $_{250\_120\_0.03}$, ID3 $_{250\_20\_0.03}$ and ID7 $_{250\_120\_0.06}$), as from an industrial point of view working at lower temperatures is more advantageous in energetic terms.

The TG and DTG curves of PUR and HCs from ID1, ID2, ID3 and ID7 are shown in Fig. 10a and b. The ignition temperature was calculated by tangent methods as shown in Fig. 10c.

The characteristic combustion parameters of PUR and HCs are reported in Table 5.

The ignition index (D_i) reported in Table 6 permits to evaluate the ignition performances of HCs. Higher values of D_i are indicative of better ignition performance [72]. Alternatively, lower *Di* indicate that the fuel is difficult to ignite [30].

From the TG curves, it can be seen that the combustion behavior of PUR changed significantly after hydrothermal processes. For PUR the $T_i = 367.6$ °C and $T_p = 546.6$ °C indicate an early onset of thermal degradation and lower thermal stability compared to the hydrochar samples.

HC from ID2 has the lowest T_i (314.8 °C), suggesting higher reactivity or lower thermal stability. Instead, HCs from ID1, ID3 and ID7 have a higher T_i than PUR, indicating enhanced thermal resistance. All the HCs exhibit a higher T_p than PUR, which implies that they combust at higher temperatures, consistent with an increasing in carbonization and aromaticity due to hydtrothermal reactions. PUR has the highest D_i value, indicating that it is faster and easier to ignite. The HCs showed lower ignition index ($D_i \leq 2.19 \times 10^{-3}$ wt%/min^3), suggesting a slow and controlled combustion process. Regarding the final temperature T_f, lower values are a clear indication of a reduced presence of unburnt compounds as for PUR; on the contrary higher T_f values as for HCs from ID1, ID3 and ID7, suggest the presence of highly stable, carbon-rich structures and slower, less efficient combustion.

4. Conclusion

This study investigates the effect of HTC and HTL operating conditions on the yields and chemical and physical properties of hydrochars derived from rigid polyurethane foam, focusing on temperature, reaction time, and feedstock to solvent ratio.

Regarding the yields, an inverse relationship is observed between severity values and HC production: as the severity value increases, the amount of solid residue tends to decrease. In contrast, an increase in the feedstock-solvent ratio does not seem to have a significant effect on HCs yields. Elemental analysis showed for all HCs a decrease in the H/C and O/C ratio that can be attributed to carbonisation, decarboxylation, dehydration and aromatization reactions and most of the obtained HCs fall into the bituminous and sub-bituminous coal region of Van Krevelen diagram. The increase in nitrogen contents showed by all the HCs, suggests their possible use as nitrogen-doped carbon materials, for the removal of water's contaminants. All the HCs showed a HHV higher than that of PUR itself (27.59 MJ/kg), and this result is indicative of an energy densification process.

The SEM analysis revealed a strong morphological dependence on reaction temperature, residence time and presence of catalyst. Reduced reaction times lead to undeveloped surfaces very similar to those of the starting feedstock, while the acidic environment favours the formation of surface micro structuring.

The combustion behaviour showed a decrease in HCs reactivity, resulting in higher ignition and peak temperatures. The HCs showed an ignition index ($D_i \leq 2.19 \times 10^{-3}$ wt%/min^3) lower than that of PUR, suggesting a slower and controlled combustion process.

Considering the liquid phases, these showed an acidic pH value close to or lower than 5. The GCMS analyses highlighted a reduction of the organic compounds present in solution in the tests obtained at high temperature (345 °C), in which the formation of variously substituted quinolines is favoured. The liquid phases of the tests carried out in acidic environment were found to be rich in organic compounds, suggesting that the acidic environment favors the formation of low molecular weight compounds and aromatic heterocyclic compounds as quinolines and isoquinolines.

These findings provide key insights to advance circular economy strategies for polyurethane waste, demonstrating that by tuning HTC and HTL operating conditions it is possible to convert PUR waste into

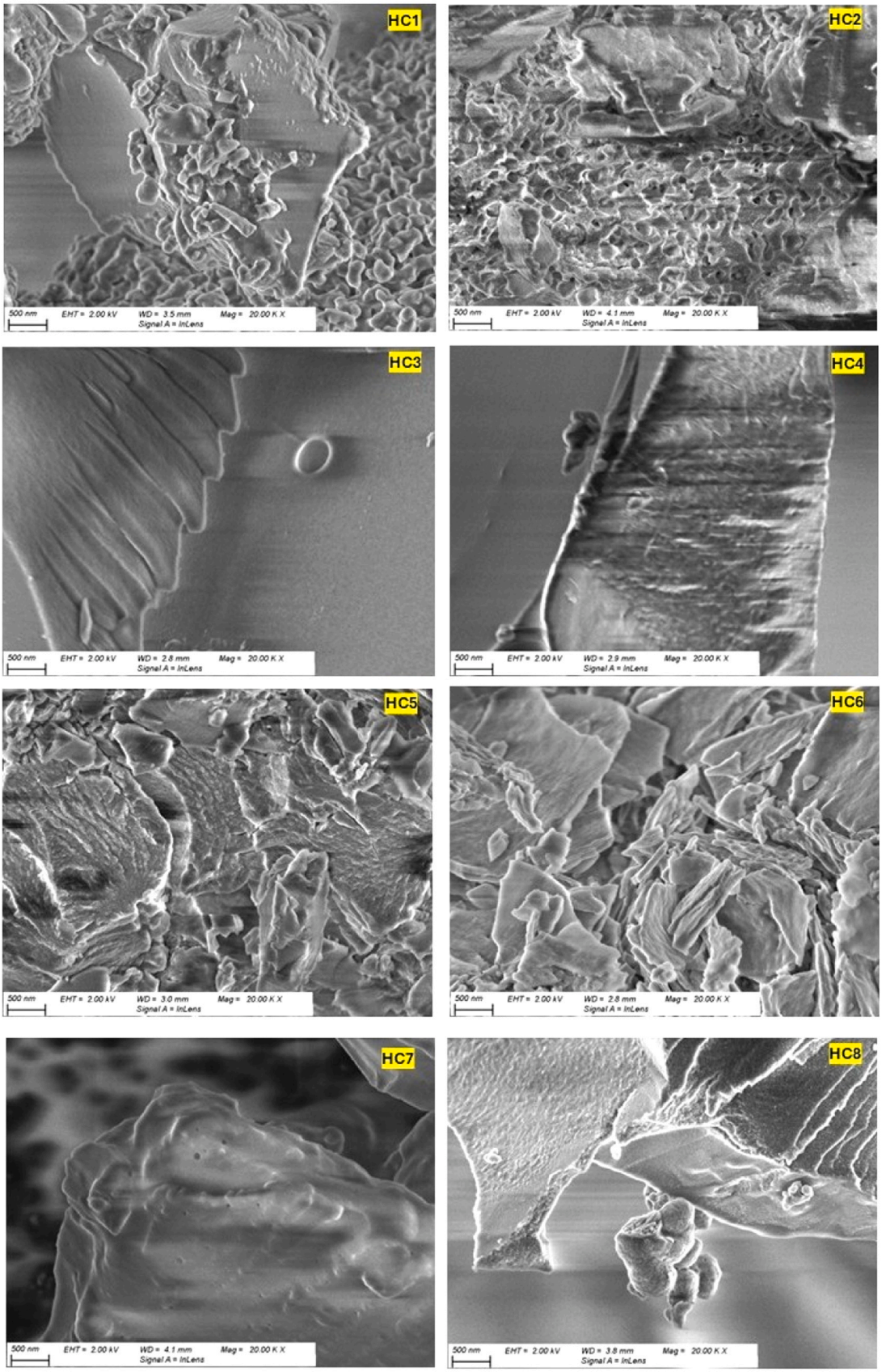

Fig. 9. SEM micrographs on HCs samples.

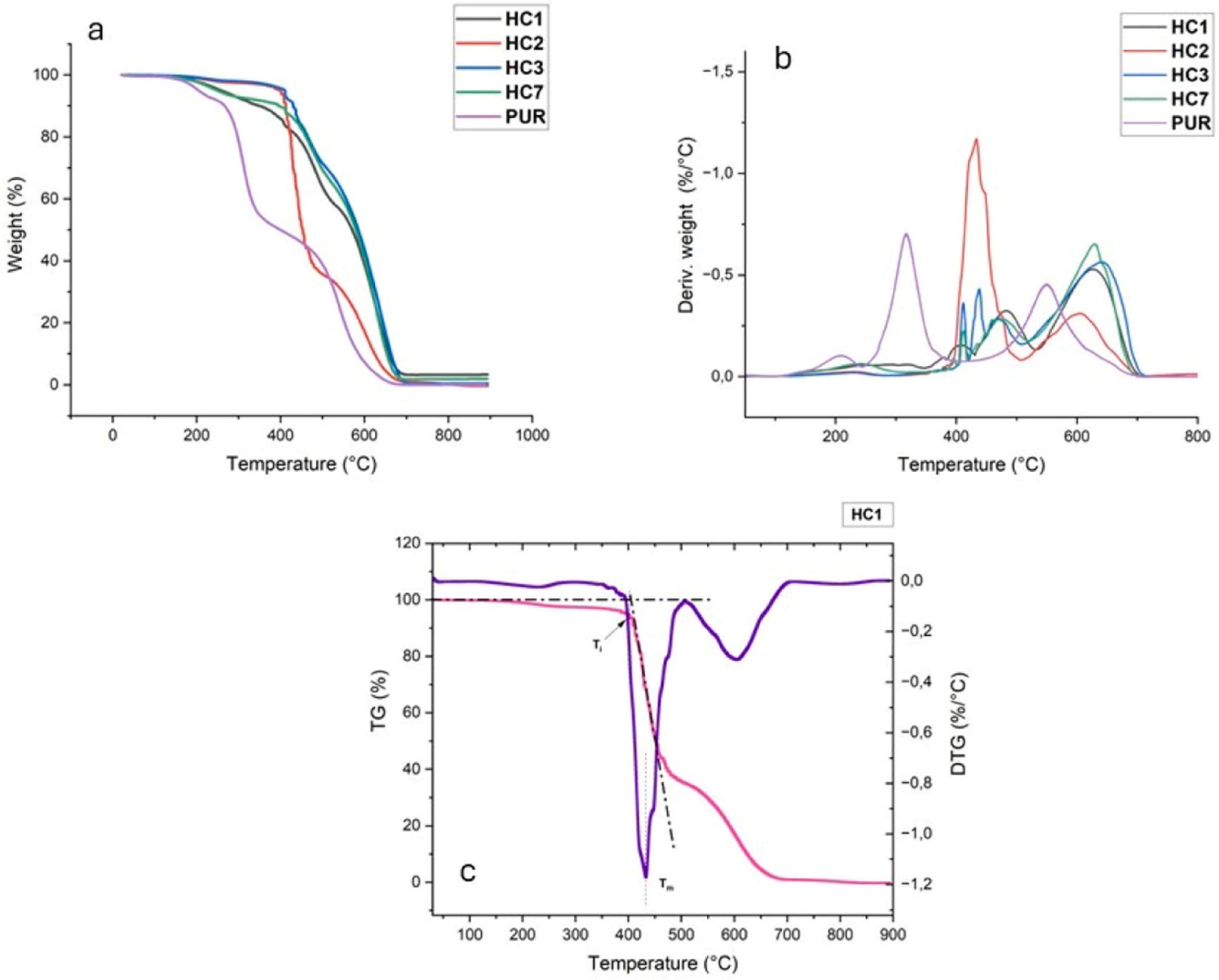

Fig. 10. TGA (a) and DTG (b) in air of HC from ID1, ID2, ID3, ID7 and PUR. Tangent method (c).

Table 5
Combustion parameters of PUR and HC ID1,2,3,7.

	T_i (°C)	T_p (°C)	T_f (°C)	D_i*10^{-3}(wt% /min^3)
PUR	367.6	546.6	635.0	2.45
HC_ID1	476.4	625.0	684.9	1.82
HC_ID2	314.8	605.2	666.0	2.19
HC_ID3	484.7	640.6	690.8	1.96
HC_ID7	502.7	628.9	680.4	2.11

valuable solid residues with suitable characteristics for use as solid fuels or nitrogen-rich materials, or enhancing the formation of liquid phases rich in molecules with potential application as platform chemicals.

CRediT authorship contribution statement

Luca Rosi: Writing – review & editing, Validation, Supervision, Project administration, Conceptualization. **Jesús Arauzo:** Writing – review & editing. **Benedetta Ciuffi:** Writing – review & editing, Writing – original draft, Methodology, Investigation, Formal analysis, Data curation, Conceptualization. **Emiliano Fratini:** Writing – review & editing, Supervision, Methodology, Conceptualization. **Edoardo Cipriani:** Investigation.

Declaration of Competing Interest

The authors declare that they have no known competing financial interests or personal relationships that could have appeared to influence the work reported in this paper.

Acknowledgements

The authors would like to thank the GPT - Thermochemical Processes Group, Zaragoza (Spain), for the feedstock characterisation. In particular Alejandro Lete, Olga Marín and Elena de la Torre. The authors thank Dr Giovanni Ferraro for conducting the scanning electron microscopy analyses.

The authors wish to thank the Fondazione Cassa di Risparmio di Firenze for financial support (ENFORCE Project, Ricercatori a Firenze, 2021 and SusFashionLab Project, 2023). EF thanks CSGI for partial financial support.

Appendix A. Supporting information

Supplementary data associated with this article can be found in the online version at doi:10.1016/j.colsurfa.2026.139868.

Data Availability

Data will be made available on request.

References

[1] A. Delavarde, G. Savin, P. Derkenne, M. Boursier, R. Morales-Cerrada, B. Nottelet, J. Pinaud, S. Caillol, Sustainable polyurethanes: toward new cutting-edge opportunities, Prog. Polym. Sci. 151 (2024) 101805, https://doi.org/10.1016/j.progpolymsci.2024.101805.

[2] PlasticsEurope. Plastics - the Facts 2024. ⟨https://plasticseurope.org/knowledge-hub/plastics-the-fast-facts-2024/⟩, 2024 (accessed 2 September 2025).

[3] R.K. Gupta, P.K. Kahol, Polyurethane Chemistry: Renewable Polyols and Isocyanates ACS Symposium Series, American Chemical Society, Washington, DC, 2021, https://doi.org/10.1021/bk-2021-1380.

[4] M.K. Chaoudhary, R.K. Gupta, Polyurethanes: An Introduction, in: ACS Symposium Series, American Chemical Society, Washington, DC, 2025, https://doi.org/10.1021/bk-2025-1507.ch001.

[5] N.V. Gama, A. Ferreira, A. Barros-Timmons, Polyurethane foams: past, present, and future, Materials 11 (2018) 1841, https://doi.org/10.3390/ma11101841.

[6] M. Ates, S. Karadag, A.A. Eker, B. Eker, Polyurethane foam materials and their industrial applications, Polym. Int. 71 (10) (2022) 1157–1163, https://doi.org/10.1002/pi.6441.

[7] E. Akdogan, M. Erdem, M.E. Ureyen, M. Kaya, Rigid polyurethane foams with halogen-free flame retardants: thermal insulation, mechanical, and flame-retardant properties, J. Appl. Polym. Sci. 137 (1) (2019) 4761, https://doi.org/10.1002/app.47611.

[8] E.A. Moawed, H.A. Kiwaan, S.K. El-Zakzouk, A. Mervat, M.A. El-Sonbati, M. Mohamed El-Zahed, Chemical recycling of polyurethane foam waste and application for antibacterial and removal of anionic and cationic dyes, Braz. J. Chem. Eng. 40 (2023) 389–401, https://doi.org/10.1007/s43153-022-00258-y.

[9] A. Kemona, M. Piotrowska, Polyurethane recycling and disposal: methods and prospects, Polymers 12 (2020) 1752, https://doi.org/10.3390/polym12081752.

[10] W. Yang, Q. Dong, S. Liu, H. Xie, L. Liu, J. Li, Recycling and disposal methods for polyurethane foam wastes, Procedia Environ. Sci. 16 (2012) 167–175, https://doi.org/10.1016/j.proenv.2012.10.023.

[11] J. Datta, M. Włoch, Polyurethane polymers. Recycling of polyurethanes, Polyurethane Polym. (2017) 323–358, https://doi.org/10.1016/B978-0-12-804039-3.00014-2.

[12] G. Rossignolo, G. Malucelli, A. Lorenzetti, Recycling of polyurethanes: where we are and where we are going, Green. Chem. 26 (2024) 1132–1152, https://doi.org/10.1039/D3GC02091F.

[13] K.Q. Tran, Process intensification and process integration for hydrothermal processing of forest residues and agricultural wastes, Waste Biorefin. (2018) 299–322, https://doi.org/10.1016/B978-0-444-63992-9.00010-0.

[14] C.A. Che, P.M. Heynderickx, Hydrothermal carbonization of plastic waste: a review of its potential in alternative energy applications, Fuel Comm. 18 (2024) 100103, https://doi.org/10.1016/j.jfueco.2023.100103.

[15] M. Plaza, C. Turner, Pressurized hot water extraction of bioactives, Trends Anal. Chem. 71 (2015) 39–54, https://doi.org/10.1016/j.trac.2015.02.022.

[16] D. Lachos-Perez, P.C. Torres-Mayanga, E.R. Abaide, G.L. Zabot, F. De Castilhos, Hydrothermal carbonization and Liquefaction: differences, progress, challenges, and opportunities, Bioresour. Technol. 343 (2022) 126084, https://doi.org/10.1016/j.biortech.2021.126084.

[17] H.D. Pham, T. Shelley, P.P. Burey, J. Feldman, A. Helwig, Hydrothermal liquefaction: a promising technology for renewable energy and environmental clean-up applications, Biomass.. Bioenergy 201 (2025) 108151, https://doi.org/10.1016/j.biombioe.2025.108151.

[18] J.Sd Passos, M. Glasius, P. Biller, Screening of common synthetic polymers for depolymerization by subcritical hydrothermal liquefaction, Process Saf. Environ. Prot. 139 (2020) 371–379, https://doi.org/10.1016/j.psep.2020.04.040.

[19] D. Hartmann, T. Rahman, L. Carias, M.L. Auad, S. Adhikari, Upcycling polyurethane plastics via thermochemical conversion pathways: a comparison of hydrothermal liquefaction and pyrolysis processes, ACS Sustain. Chem. Eng. 12 (42) (2024) 15515–15527, https://doi.org/10.1021/acssuschemeng.4c05202.

[20] H. Wang, H. Gupta, N.R. Shiju, Recycling of polyurethane waste: facile hydrothermal conversion using acidic and basic additives, ChemSusChem 19 (2025) 1, https://doi.org/10.1002/cssc.202502372.

[21] G. Widanagamage, Z. Zhang, I.M. O'Hara, L. Moghaddam, Recycling biobased polyurethane foams: efficient dual recovery of polyols and diamines via hydrothermal liquefaction, Chem. Eng. J. 523 (2025) 168533, https://doi.org/10.1016/j.cej.2025.168533.

[22] W. Chen, G. Zhang, D. Li, S. Ma, B. Wang, X. Jiang, Preparation of nitrogen-doped porous carbon from waste polyurethane foam by hydrothermal carbonization for H_2S adsorption, Ind. Eng. Chem. Res. 59 (16) (2020) 7447–7456, https://doi.org/10.1021/acs.iecr.0c00498.

[23] J. Duan, B. Zhang, H. Fan, W. Shen, S. Qu, Nitrogen-doped carbon nanosheets from polyurethane foams and removal of Cr(VI), Carbon Lett. 22 (2017) 60–69, https://doi.org/10.5714/cl.2017.22.060.

[24] X. Liu, Z. Geng, Y. Sun, W. Sun, Polyurethane-converted activated carbons with tailorable porosity and surface functionality for supercapacitors, J. Energy Storage (2025) 115988, https://doi.org/10.1016/j.est.2025.115988.

[25] R. Gallorini, B. Ciuffi, F. Real Fernandez, C. Carozzini, E. Ravera, A.M. Papini, L. Rosi, Subcritical hydrothermal liquefaction as a pretreatment for enzymatic degradation of polyurethane, ACS Omega 7 (42) (2022) 37757–37763, https://doi.org/10.1021/acsomega.2c04734.

[26] G. Haarlemmer, L. Matricon, A. Roubaud, Comprehensive review of hydrothermal liquefaction data for use in machine-learning models, BioFPR 18 (5) (2024) 1782–1798, https://doi.org/10.1002/bbb.2637.

[27] E. Takatori, N. Kagawa, Analysis of additives in plastics, Int. Polym. Sci. Tech. 34 (3) (2007) 11–16, https://doi.org/10.1177/0307174X0703400302.

[28] M. Kalivodová, M. Baláš, P. Milčák, H. Lisá, M. Lisý, J. Lachman, P. Kracík, P. Križan, K. Vejražka, The determination of higher heating value by calculation based on elemental analysis, Paliva 14 (1) (2022) 8–20, https://doi.org/10.35933/paliva.2022.01.02.

[29] A.D. Glova, Y. Miao, S. Yoshizaki, Relationship between heating value and chemical composition of selected agricultural and forest biomass, Jpn. J. Trop. Agr. 38 (1) (1994) 1–7, https://doi.org/10.11248/jsta1957.38.1.

[30] X. Zhao, L. Zhan, B. Xie, B. Gao, Products derived from waste plastics (PC, HIPS, ABS, PP and PA6) via hydrothermal treatment: characterization and potential applications, Chemosphere 207 (2018) 742–752, https://doi.org/10.1021/acsomega.2c00522.

[31] Y. Zhang, Y. Guo, F. Cheng, K. Yan, Y. Cao, Investigation of combustion characteristics and kinetics of coal gangue with different feedstock properties by thermogravimetric analysis, Thermochim. Acta 614 (20) (2015) 137–148, https://doi.org/10.1016/j.tca.2015.06.018.

[32] B.G. Ma, X.-G. Li, L. Xu, K. Wang, X.-G. Wang, Investigation on catalyzed combustion of high ash coal by thermogravimetric analysis, Thermochim. Acta 445 (2006) 19–22, https://doi.org/10.1016/j.tca.2006.03.021.

[33] S. Aich, D. Behera, B.K. Nandi, S. Bhattachary, Relationship between proximate analysis parameters and combustion behaviour of high ash Indian coal, Int J. Coal Sci. Technol. 7 (2020) 766–777, https://doi.org/10.1007/s40789-020-00312-5.

[34] L. Tang, J. Xiao, Q. Mao, Z. Zhang, Z. Yao, X. Zhu, S. Ye, Q. Zhong, Thermogravimetric analysis of the combustion characteristics and combustion kinetics of coals subjected to different chemical demineralization processes (https://pubs.acs.org/doi/), ACS Omega 7 (16) (2022) 13998–14008, https://doi.org/10.1021/acsomega.2c00522.

[35] M. Szycher Ph.D. Szycher's Handbook of Polyurethanes, Second edition, CRC Press, (USA), 2017, https://doi.org/10.1201/b12343.

[36] H. Lim, S.H. Kim, B.K. Kim, Effects of the hydroxyl value of polyol in rigid polyurethane foams, Polym. Adv. Technol. 19 (12) (2008) 1729–1734, https://doi.org/10.1002/pat.1188.

[37] R. Van Maris, Y. Tamano, H. Yoshimura, K.M. Gay, Polyurethane catalysis by tertiary amines, J. Cell. Plast. 41 (4) (2005) 305–322, https://doi.org/10.1177/0021955X0505511.

[38] J.A. Galbis, M. de, G. García-Martín, M.V. de Paz, E. Galbis, Bio-based polyurethanes from carbohydrate monomers, in: Aspects of Polyurethanes, InTech, 2017, https://doi.org/10.5772/intechopen.69606.

[40] T. Reissner, A. Panchenko, C. Renner, S. Zarbakhsh, Amine Catalyst for the Production of Polyurethanes, DPMA Deutsches Patent- und Markenamt, 2017. ⟨https://patents.google.com/patent/DE102017203271A1/en⟩. Patent No: DE102017203271A1.

[41] H. Plaisance, G. Raffy, B. Le Bot, E. Bossanne, C. Rawas, P. Cardin, V. Desauziers, Characteristics of Tris(chloropropyl)phosphate (TCPP) emission from upholstered furniture in offices and consequence on indoor air quality, Build. Environ. 219 (2022) 109156, https://doi.org/10.1016/j.buildenv.2022.109156.

[42] ECHA (European Chemicals Agency) Screening report an assessment of whether the use of TCEP, TCPP and TDCP in articles should be restricted Annex XV reporting format 040615 (europa.eu), (2018), ⟨https://echa.europa.eu/documents/10162/13641/screening_report_tcep_tcpp_td-cp_en.pdf/e0960aa7-f703-499c-24ff-fba627060698⟩. Accessed 27.01.2025.

[43] B.L. Wadey, Plasticizers, Encycl. Phys. Sci. Technol. (2003) 441–456, https://doi.org/10.1016/B0-12-227410-5/00586-X.

[44] H. Stančin, H. Mikulčić, N. Manić, D. Stojiljiković, M. Vujanović, X. Wang, N. Duić, Thermogravimetric and kinetic analysis of biomass and polyurethane foam mixtures co-pyrolysis, Energy 237 (15) (2021) 121592, https://doi.org/10.1016/j.energy.2021.121592.

[45] H. Stančin, J. Růžičková, H. Mikulčić, H. Raclavská, M. Kucbel, X. Wang, N. Duić, Experimental analysis of waste polyurethane from household appliances and its utilization possibilities, J. Environ. Manag. 243 (2019) 105–115, https://doi.org/10.1016/j.jenvman.2019.04.112.

[46] R. Gómez-Rojo, L. Alameda, Á. Rodríguez, V. Calderón, S. Gutiérrez-González, Characterization of polyurethane foam waste for reuse in eco-efficient building materials, Polymers 11 (2019) 359, https://doi.org/10.3390/polym11020359.

[47] I. Beverte, U. Cabulis, J. Andersons, M. Kirpluks, V. Skruls, P. Cabulis, Light microscopy of medium-density rigid polyurethane foams filled with nanoclay, Polymers 14 (2022) 1154, https://doi.org/10.3390/polym14061154.

[48] D. Baillis, R. Coquard, Radiative and conductive thermal properties of foams, in: A. Öchsner, G.E. Murch, M.J.S. de Lemos (Eds.), Cellular and Porous Materials: Thermal Properties Simulation and Prediction, Wiley-VCH, Weinheim, 2008, pp. 343–384, https://doi.org/10.1002/9783527621408.ch11.

[49] D. Egesa, P. Mulindwa, E. Mubiru, H.D. Kyomuhimbo, G. Aturagaba, Hydrothermal liquefaction of water hyacinth: effect of process conditions and magnetite nanoparticles on biocrude yield and composition, J. Sustain. Bioenergy Syst. 11 (2021) 157–186, https://doi.org/10.4236/jsbs.2021.114012.

[50] Y. Zhang, Q. Jiang, W. Xie, Y. Wang, J. Kang, Effects of temperature, time and acidity of hydrothermal carbonization on the hydrochar properties and nitrogen recovery from corn stover, Biomass.. Bioenergy 122 (2019) 175–182, https://doi.org/10.1016/j.biombioe.2019.01.035.

[51] H. Mumtaz, S. Sobek, S. Werle, M. Sajdak, R. Muzyka, Hydrothermal treatment of plastic waste within a circular economy perspective, Sustain Chem. Pharm. 32 (2023) 100991, https://doi.org/10.1016/j.scp.2023.100991.
[52] B.J. He, Y. Zhang, Y. Yin, T.L. Funk, G.L. Riskowski, Preliminary characterization of raw oil products from the thermochemical conversion of swine manure, Trans. ASAE 44 (6) (2001) 1865–1871, https://doi.org/10.13031/2013.7025.
[53] Z. Zhang, J. Yang, J. Qian, Y. Zhao, T. Wang, Y. Zhai, Biowaste hydrothermal carbonization for hydrochar valorization: skeleton structure, conversion pathways and clean biofuel applications, Bioresour. Technol. 324 (2021) 124686, https://doi.org/10.1016/j.biortech.2021.124686.
[54] S. Román, J. Nabais, C. Laginhas, B. Ledesma, J. González, Hydrothermal carbonization as an effective way of densifying the energy content of biomass, Fuel Process. Technol. 103 (2012) 78–83, https://doi.org/10.1016/j.fuproc.2011.11.009.
[55] A. Jeder, A. Sanchez-Sanchez, P. Gadonneix, E. Masson, A. Ouederni, A. Celzard, V. Fierro, The severity factor as a useful tool for producing hydrochars and derived carbon materials, Environ. Sci. Pollut. Res. Int. 25 (2) (2018) 1497–1507, https://doi.org/10.1007/s11356-017-0366-7.
[56] H.A. Ruiz, R.M. Rodríguez-Jasso, B.D. Fernandes, A.A. Vicente, J.A. Teixeira, Hydrothermal processing, as an alternative for upgrading agriculture residues and marine biomass according to the biorefinery concept: a review, Renew. Sustain. Energy Rev. 21 (2013) 35–51, https://doi.org/10.1016/j.rser.2012.11.069.
[57] M. Volpe, L. Fiori, From olive waste to solid biofuel through hydrothermal carbonisation: the role of temperature and solid load on secondary char formation and hydrochar energy properties, JAAP 124 (2017) 63–72, https://doi.org/10.1016/j.jaap.2017.02.022.
[58] A.T. Tag, G. Duman, J. Yanik, Influences of feedstock type and process variables on hydrochar properties, Bioresour. Technol. 250 (2018) 337–344, https://doi.org/10.1016/j.biortech.2017.11.058.
[59] G. Collin, H. Höke, Quinoline and Isoquinoline. Ullmann's Encyclopedia of Industrial Chemistry, Wiley-VCH, 2000, pp. 1–5, https://doi.org/10.1002/14356007.a22_465.
[60] A. Funke, F. Ziegler, Hydrothermal carbonization of biomass: a summary and discussion of chemical mechanisms for process engineering, BioFPR 4 (2) (2010) 160–177, https://doi.org/10.1002/bbb.198.
[61] J.R. Laszakovits, A.A. MacKay, Data-based chemical class regions for Van Krevelen diagrams, J. Am. Soc. Mass Spectrom. 33 (2022) 198–202, https://doi.org/10.1021/jasms.1c00230.
[62] K. Daegi, K. Lee, K.Y. Park, Hydrothermal carbonization of anaerobically digested sludge for solid fuel production and energy recovery, Fuel 130 (2014) 120–125, https://doi.org/10.1016/j.fuel.2014.04.030.
[63] Md.T. Islam, M.T. Reza, Evaluation of fuel and combustion properties of hydrochar derived from Co-hydrothermal carbonization of biomass and plastic, Biomass.. Bioenergy 172 (2023) 106750, https://doi.org/10.1016/j.biombioe.2023.106750.
[64] M. Śliz, M. Wilk, A comprehensive investigation of hydrothermal carbonization: Energy potential of hydrochar derived from Virginia mallow, Renew. Energy 156 (2020) 942–950, https://doi.org/10.1016/j.renene.2020.04.124.
[65] M. Hejna, K. Świechowski, W.A. Rasaq, A. Białowiec, Study on the effect of hydrothermal carbonization parameters on fuel properties of chicken manure hydrochar, Materials 15 (16) (2022) 5564, https://doi.org/10.3390/ma15165564.
[66] C.I. Aragón-Briceño, O. Grasham, A.B. Ross, V. Dupont, M.A. Camargo-Valero, Hydrothermal carbonization of sewage digestate at wastewater treatment works: Influence of solid loading on characteristics of hydrochar, process water and plant energetics, Renew. Energy 157 (2020) 959–973, https://doi.org/10.1016/j.renene.2020.05.021.
[67] S.Z. Roslan, S.F. Zainudin, A. Mohd Aris, K.B. Chin, M. Musa, A.R. Mohamad Daud, S.S.A. Syed Hassan, Hydrothermal carbonization of sewage sludge into solid biofuel: influences of process conditions on the energetic properties of hydrochar, Energies 16 (2023) 2483, https://doi.org/10.3390/en16052483.
[68] G. Altiparmaki, M.A. Vasileiadou, S. Vakalis, The effect of excess water on the hydrothermal carbonization of anise waste from ouzo production on Lesvos Island, Sustain. Chem. Pharm. 29 (2022) 100831, https://doi.org/10.1016/j.scp.2022.100831.
[69] M. Lucian, M. Volpe, L. Gao, G. Piro, J.L. Goldfarb, L. Fiori, Impact of hydrothermal carbonization conditions on the formation of hydrochars and secondary chars from the organic fraction of municipal solid waste, Fuel 233 (2018) 257–268, https://doi.org/10.1016/j.fuel.2018.06.060.
[70] S. Abel, A. Peters, S. Trinks, H. Schonsky, M. Facklam, G. Wessolek, Impact of biochar and hydrochar addition on water retention and water repellency of sandy soil, Geoderma 202–203 (2013) 183–191, https://doi.org/10.1016/j.geoderma.2013.03.003.
[71] T. Wang, Y. Zhai, Y. Zhu, C. Li, G. Zeng, A review of the hydrothermal carbonization of biomass waste for hydrochar formation: Process conditions, fundamentals, and physicochemical properties, Renew. Sustain. Energy Rev. 90 (2018) 223–247, https://doi.org/10.1016/j.rser.2018.03.071.
[72] Z. Liu, A. Quek, S. Kent Hoekman, R. Balasubramanian, Production of solid biochar fuel from waste biomass by hydrothermal carbonization, Fuel 103 (2013) 943–949, https://doi.org/10.1016/j.fuel.2012.07.069.